CYCLONE GLOBAL NAVIGATION SATELLITE SYSTEM (CYGNSS)

Algorithm Theoretical Basis Document Level 2 Mean-Square Slope Retrieval		
	UM Doc. No.	**148-0139**
	SwRI Doc. No.	**N/A**
	Revision	**3**
	Date	**22 September 2016**
	Contract	**NNL13AQ00C**

Algorithm Theoretical Basis Documents (ATBDs) provide the physical and mathematical descriptions of the algorithms used in the generation of science data products. The ATBDs include a description of variance and uncertainty estimates and considerations of calibration and validation, exception control and diagnostics. Internal and external data flows are also described.

SPACE PHYSICS RESEARCH LABORATORY

SwRI

NASA

CYCLONE GLOBAL NAVIGATION SATELLITE SYSTEM (CYGNSS)

Algorithm Theoretical Basis Document Level 2 Mean-Square Slope Retrieval		
	UM Doc. No.	**148-0139**
	SwRI Doc. No.	**N/A**
	Revision	**3**
	Date	**22 Sept 2016**
	Contract	**NNL13AQ00C**

Prepared by: Valery Zavorotny, NOAA/ESRL
Chris Ruf, University of Michigan

Approved by: *Email approval on file* Date: 28 Sep 2016
John Scherrer, CYGNSS Project Manager

Approved by: *Email approval on file* Date: 28 Sep 2016
Randy Rose, CYGNSS Project Systems Engineer

Released by: *Email approval on file* Date: 28 Sep 2016
Damen Provost, CYGNSS UM Project Manager

SPACE PHYSICS RESEARCH LABORATORY

NASA

REVISION NOTICE

Document Revision History		
Revision	**Date**	**Changes**
PRE-RELEASE DRAFT	17 June 2013	n/a
INITIAL RELEASE	24 December 2013	Add explicit relationship between MSS and the Level 1 BRCS data product.
REVISION 1	13 April 2014	Add description of ancillary data requirements; Expand error analysis
REVISION 2	22 April 2014	Update links to ancillary data sources
REVISION 3	22 September 2014	Add explicit algorithm to determine the uncertainty in each MSS estimate (Section 4.3)

Table of Contents

1. Introduction and Background

1.1 Introduction

The primary mission of the CYGNSS Project is to collect measurements of ocean surface winds through variations in the direct vs. reflected Global Positioning System (GPS) signals. It will be achieved through fitting the calibrated data obtained by the CYGNSS eight microsatellite observatories to the empirical or modeled functions which relate the measured signal parameters, e.g., the Delay-Doppler Map (DDM) peak power, to surface wind. At the same time, such an ocean surface characteristic as the mean-square slope (MSS) will be also available.

Within the framework of the scattering model adopted here the MSS can be related directly to the bistatic radar cross section σ_0. On the other hand, the bistatic radar equation allows connecting σ_0 to the calibrated estimates of power for each delay/Doppler bin through the instrument calibration algorithm. The algorithm theory is based on the details of the instrument processing chain hardware and firmware, a model of the received signal power model [1], and estimates of the external and internally generated noise power. The purpose of this document is to describe the CYGNSS Level 2 mean-square slope algorithms and provide all necessary equations for implementing the algorithm during the mission. Sub-section 1.2 provides science background and objectives. It explains the need for ocean mean-square slope (MSS). Section 2 describes the physics of the problem and explains the connection between the bistatic radar cross section and the MSS, and between the MSS and the ocean surface spectrum. Section 3 provides an overview of the MSS retrieval algorithm.

1.2 Science Background and Objectives

1.2.1 Need for Ocean Mean Square Slope (MSS)

The MSS of the ocean surface is a very important quantity. It is crucial for understanding the physical processes at the air–sea interface, and for interpreting altimeter and scatterometer radar backscatter measurements [2-7]. The need for global MSS data sets in air-sea interaction research is increasingly apparent. Indeed, the presence of waves significantly enhances gas transfer rates across a water boundary layer. The transfer rates correlate well with the mean-square slope of the waves. It has been observed in laboratory conditions that gas transfer velocities significantly increase at the onset of surface wave generation [2].

The need for ocean MSS is also evident in satellite radiometry, specifically for salinity measurements [8, 9]. At L-band, the brightness temperature of the ocean surface depends equally on three surface parameters: the sea surface salinity, the sea surface temperature and the sea state, which is responsible for the deviations of the brightness temperature with respect to the flat sea model. To estimate the sea roughness effect on brightness temperature various models driven either directly by 10-m-height wind speed, U_{10}, or by the significant wave height (SWH) have been tried without significant success. With the advent of the GNSS-R technique which uses L-band signals the idea has been proposed to measure L-band limited MSS to provide sea surface roughness estimates for L-band radiometric measurements of ocean salinity [9, 8].

2 Physics of the Problem

2.1 Connection between the Bistatic Radar Cross Section and the MSS

According to the forward model based on the bistatic radar equation adopted for the case of the GNSS scattered signals, the DDM emerges as a result of the integration of the product of several factors over a certain ocean surface area. One of those factors is the normalized ocean bistatic radar cross section (BRCS) σ_0 which describes the effect of ocean surface roughness. In the geometric-optics limit of the Kirchhoff approximation this term is represented by the following expression [10, 11]:

$$\sigma_0 = \pi \left|\Re\right|^2 \left(q / q_z\right)^4 P\left(-q_\perp / q_z\right), \tag{2.1}$$

where $\vec{q}$ is the scattering vector which can be regarded as a function of the coordinate $\vec{\rho}$ in the mean surface plane; $\Re$ is the complex Fresnel coefficient, which depends on signal polarization state, a complex dielectric constant of the reflecting medium, ε, and the local incidence angle. In the case of GNSS-R, the polarization state of the reflected signal is left-hand circular polarization (LHCP). The factor $P(\vec{s})$ in (2.1) is the probability density function (PDF) of large-scale "smoothed" surface slopes. The adjective "smoothed" implies that very small-scale components of the surface spectrum (of the order of several tens of centimeters) are filtered out. This is a consequence of using in this technique 0.2 m-long L-band waves which obey the geometric-optics limit of the Kirchhoff approximation. In order to sense all surface scales one would need to use 1 mm (or shorter) EM waves.

It is believed that for linear surface gravity waves the slope PDF $P(\vec{s})$ can be approximated by the anisotropic bivariate Gaussian distribution [1, 12-13] which for the case of wind directed along *x*- or *y*-axis is:

$$P(\vec{s}) = \frac{1}{2\pi\sqrt{mss_x mss_y (1-b_{x,y}^2)}} \exp\left[-\frac{1}{2(1-b_{x,y}^2)}\left(\frac{s_x^2}{mss_x} - 2b_{x,y}\frac{s_x s_y}{\sqrt{mss_x mss_y}} + \frac{s_y^2}{mss_y}\right)\right]. \tag{2.2}$$

where mss_x and mss_y are mean-square slopes of the sea surface for two orthogonal components, one is along the wind direction, and another is across it; $b_{x,y}$ is the correlation coefficient between two slope components. Upon substitution of (2.2) into (2.1) we obtain an algebraic expression that connects the MSS components with the BRCS, σ_0:

$$\sigma_0(\vec{q}) = \frac{\left|\Re\right|^2 \left(q / q_z\right)^4}{2\sqrt{mss_x mss_y (1-b_{x,y}^2)}} \exp\left[-\frac{1}{2q_z^2(1-b_{x,y}^2)}\left(\frac{q_x^2}{mss_x} - \frac{2b_{x,y}q_x q_y}{\sqrt{mss_x mss_y}} + \frac{q_y^2}{mss_y}\right)\right]. \tag{2.3}$$

2.2 Connection between the MSS and the surface elevation spectrum

By definition, the MSS components are introduced as

$$mss_{x,y} = \left\langle s_{x,y}^2 \right\rangle = \iint\limits_{\kappa<\kappa_*} \kappa_{x,y}^2 \Psi\left(\vec{\kappa}\right) d^2\kappa ; \tag{2.4}$$

$$b_{x,y} = \left\langle s_x s_y \right\rangle / \sqrt{mss_x mss_y} ; \tag{2.5}$$

$$\left\langle s_x s_y \right\rangle = \iint\limits_{\kappa<\kappa_*} \kappa_x \kappa_y \Psi\left(\vec{\kappa}\right) d^2\kappa . \tag{2.6}$$

Therefore, two MSS components, mss_x and mss_y are determined solely by the wave-number integral from the ocean elevation spectrum $\Psi(\vec{\kappa})$ times $\kappa_{x,y}^2$. This product is called a slope spectral density. The limit of integration at low wavenumbers is κ_*, which plays a role as the "smoothing" filter which is related to the EM wave length and the angle of incidence. There are some indications that the actual PDF of slopes does not exactly follow a Gaussian shape at their tails [14]. In terms of the glistening zone, it implies that this departure affects the periphery of the zone. However, for the conditions of the CYGNSS mission, most of the contribution to the signal comes from the peak area of the PDF of slopes. Frequently, when it is not possible to measure each of two orthogonal components, the total MSS is used:

$$mss = \left\langle s^2 \right\rangle = \left\langle s_x^2 \right\rangle + \left\langle s_y^2 \right\rangle = mss_x + mss_y = \iint\limits_{\kappa<\kappa_*} \kappa^2 \Psi\left(\vec{\kappa}\right) d^2\kappa . \tag{2.7}$$

In the case of global winds, the model spectrum $\Psi(\vec{\kappa})$ proposed by Elfouhaily et al. [15] is widely used. An example of the Elfouhaily et al. slope spectrum taken along the wind direction is shown in Fig. 2.1

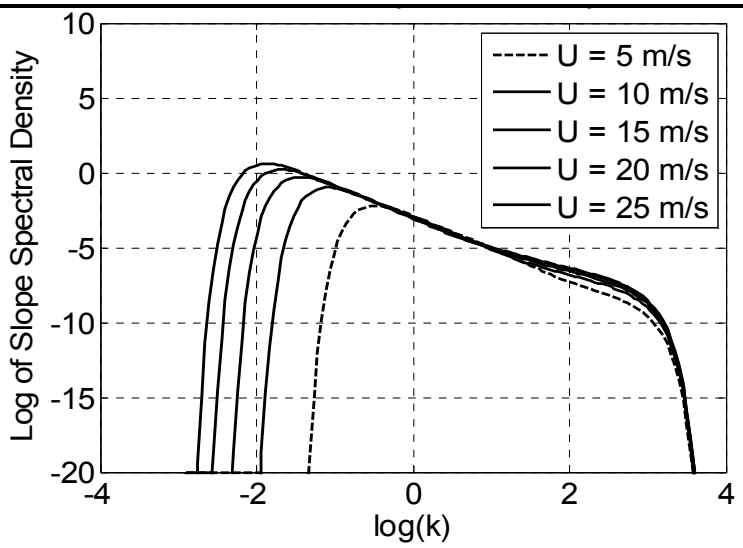

Fig. 2.1 Ocean surface slope spectrum from [15] taken along the wind direction.

This empirical model describes deep-water waves driven by winds of constant direction under diverse wave-age (often called 'fetch') conditions. This model has two input parameters, the local wind speed at 10-m height, U_{10}, and the wave age, or fetch. It was designed to agree with *in situ* observations of the first sun-glint derived wave slope measurements of Cox and Munk [16], performed several decades ago.

For conditions when the surface can be described by the Elfouhaily et al. spectrum (assuming that the fetch is known) it is possible to retrieve the wind U_{10} from the CYGNSS measurement. At the same time, the retrieval of the total MSS is available as a byproduct of the wind retrieval. In some cases, the total MSS retrieval may be the only product which has a high level of validity. This may occur when sea roughness cannot be described solely by the local wind (e.g. in the presence of unknown swell, currents, surfactants, etc.) so the surface cannot be described by the Elfouhaily et al. spectrum or its proxy. For example, if swell is present which does not interact with the waves driven by the local wind then the total spectrum of the wave will be

$$\Psi_{tot}\left(\vec{\kappa}\right) = \Psi_{wind}\left(\vec{\kappa}\right) + \Psi_{swell}\left(\vec{\kappa}\right) \tag{2.8}$$

And the total MSS component will obey the equation:

$$mss_{x,y,tot} = mss_{x,y,wind} + mss_{x,y,swell} \tag{2.9}$$

As was pointed out above, the mean-square slope that determines the BRCS through the PDF of slopes is not a full-wave slope. Even though the sea surface contains wave harmonic components both longer and shorter than the L-band electromagnetic waves, the short waves can be disregarded in a process of forward quasi-specular reflection under the geometric optics approximation. Therefore, the full surface spectrum should be cut off at the high end of wave numbers. There are

various choices of cutoff wave number κ_* which are discussed in the Section 4.2 "Rough Surface Scattering" of the ATBD Level 2 Wind Speed Retrieval [17].

3. Retrieval Algorithm Overview

3.1 Theoretical Description

Since the regime of CYGNSS measurements does not allow one to distinguish between the along- and cross- wind directions, we assume that $mss_y = mss_x = mss/2$, and $b_{x,y}^2 = 0$. Then, the expression for the bistatic radar cross section from (2.3) simplifies:

$$\sigma_0(\vec{q}) = \frac{|\Re|^2}{mss}\left(\frac{q}{q_z}\right)^4 \exp\left(-\frac{q_\perp^2}{q_z^2 mss}\right) \tag{3.1}$$

Factors containing components of the scattering vector $\vec{q}$ can be expressed through local (at the point of reflection) incidence and scattering angles, θ_1 and θ_2 (see Fig. (3.1)).

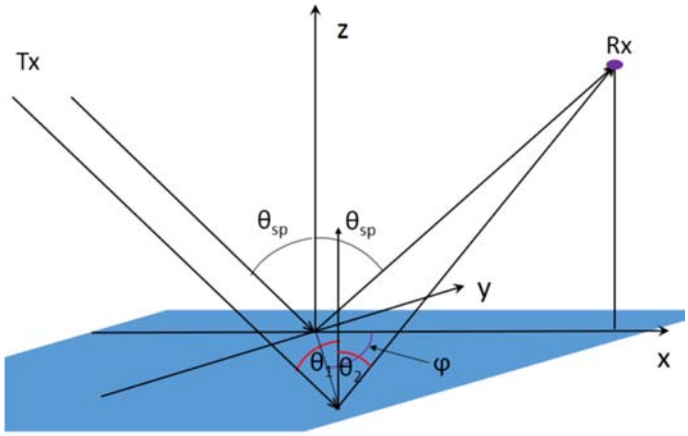

Fig. 3.1. Geometry of quasi-specular scattering

$$\left(\frac{q}{q_z}\right)^2 = \frac{2\left(1-\sin\theta_1\sin\theta_2\cos\varphi+\cos\theta_1\cos\theta_2\right)}{\left(\cos\theta_1+\cos\theta_2\right)^2}, \tag{3.2}$$

$$\frac{q_\perp^2}{q_z^2} = \frac{\left(\sin\theta_2\cos\varphi-\sin\theta_1\right)^2+\sin^2\theta_2\sin^2\varphi}{\left(\cos\theta_1+\cos\theta_2\right)^2}. \tag{3.3}$$

In principle, MSS can be retrieved from (3.1) for any combination of incident and scattering angles θ_1 and θ_2 (and azimuthal scattering angle φ) by solving a transcendental equation

$$\log mss - \frac{q_\perp^2}{q_z^2 mss} - \log\left[\left|\Re\right|^2\left(\frac{q}{q_z}\right)^4\right] + \log\sigma_0\left(\vec{q}\right) = 0\,. \qquad (3.4)$$

However, more beneficial would be to use $\sigma_0(\theta)$ in the specular direction where $\theta_1 = \theta_2 = \theta$, and $\varphi = 0$. Then, (3.1) simplifies to

$$\sigma_0(\theta) = \frac{\left|\Re(\theta)\right|^2}{mss}, \qquad (3.5)$$

The Fresnel reflection coefficient of the ocean surface, $\Re$, is evaluated in the nominal specular direction described by the incidence angle θ.

3.2 Baseline Algorithm

In [17], an equation was obtained which expresses BRCS σ_0 through available calibrated measured power values from the Level 1A calibration described elsewhere and parameters of the system:

$$\sigma_0 = \alpha \overline{P}^{Sig}_{\hat{\tau},\hat{f}}\,, \qquad (3.6)$$

where α is a coefficient which depends on various geometric, transmitter and receiver parameters:

$$\alpha = \frac{(4\pi)^3 R_T^2 R_R^2 L^1_{atm} L^2_{atm}}{P_T T_i^2 \lambda^2 G_T G_R \chi_{\hat{\tau},\hat{f}}} \qquad (3.7)$$

where:

1) $\overline{P}^{Sig}_{\hat{\tau},\hat{f}}$ is the calibrated Level 1A DDM, as a function of delay and frequency;
2) R_T is the GPS transmitter to specular point path length, calculated using the IGS positions of the GPS satellites and estimated specular point location;
3) R_R is the specular point to CYGNSS satellite path length, calculated using the positions of the CYGNSS spacecraft and estimated specular point location;
4) L^1_{atm} and L^2_{atm} are the atmospheric losses as the signal travels from the GPS satellite to the surface, and from the surface to the receiver, respectively. These terms will be estimated on the ground using a propagation model at the GPS signal transmit frequency;
5) P_T is the GPS transmit signal power and is estimated using the absolute power of the direct signal;
6) T_i is the coherent time integration;
7) λ is the signal wavelength;
8) G_T is the GPS antenna gain for the reflection geometry. This will be calculated using a model of the GPS antenna gain pattern generated using power measurements from the direct signal.

The above two terms will be estimated together as a single combined quantity;

9) G_R is the CYGNSS Nadir antenna gain, which is a function of reflection geometry and S/C orientation. This term will be estimated using a pre-launch calibration of the antenna pattern and the reflection viewing geometry;

10) $\chi_{\hat{\tau},\hat{f}}$ is the effective scattering area for the delay- Doppler bin at $\hat{\tau},\hat{f}$. This area will be estimated based on the delay-Doppler surface geometry calculated using modules within the CYGNSS end-to-end simulator (E2ES).

Details for the calculation of each of the above terms are described in [17].

For the CYGNSS geometry and system parameters, the coefficient $\alpha \approx 10$ at $\theta = 35^\circ$ for the DDM bin with $\hat{\tau} = 0,\ \hat{f} = 0$ which corresponds to a nominal specular point on the surface. The MSS estimation algorithm is found by solving for MSS in Eq. (3.5), or

$$mss = \frac{\left|\Re(\theta)\right|^2}{\sigma_0(\theta)} \tag{3.8}$$

where $\Re$ is the Fresnel reflection coefficient evaluated at the incidence angle of the specular point, for a given complex dielectric constant of the ocean surface ε. Thus, the MSS estimation error is determined by uncertainties of several parameters entering (3.8). Two leading parameters are bistatic radar cross section (BRCS), σ_o, provided by the Level 1 DDM Calibration Algorithm [17], and the absolute value squared of the Fresnel reflection coefficient $\left|\Re(\theta)\right|^2$. In turn, the Fresnel reflection coefficient is determined by the complex dielectric constant, ε, of the ocean surface and the incidence angle at the specular point. Estimation of ε requires knowledge of the sea surface temperature and salinity. Related uncertainties will be analyzed in the next Section.

4. Performance Characterization

4.1 Accuracy

If we put aside the issue of geophysical variability of the mean square slope of ocean waves, the accuracy of the MSS retrieval based on (3.8) is determined by the uncertainty in two factors entering (3.8), bistatic radar cross section (BRCS) σ_0 taken in the specular direction, and the absolute-value-squared of the Fresnel reflection coefficient of the flat ocean surface, $|\Re(\theta)|^2$ also taken in the specular direction. The analysis of the σ_0 uncertainty is done in [17]. It boils down to two numbers.

Let us, first start with estimation of accuracy of the reflection coefficient. In the case of left-hand circular polarization (LHCP), the expression for the complex Fresnel reflection coefficient $\Re$ at the interface between air and a medium (in our case, sea water) with a complex dielectric permittivity ε, is:

$$\Re(\theta)=\frac{1}{2}\left[\frac{\varepsilon\cos\theta-\sqrt{\varepsilon-\sin^2\theta}}{\varepsilon\cos\theta+\sqrt{\varepsilon-\sin^2\theta}}-\frac{\cos\theta-\sqrt{\varepsilon-\sin^2\theta}}{\cos\theta+\sqrt{\varepsilon-\sin^2\theta}}\right] \tag{4.1}$$

where θ is the local incidence (or reflection) angle. We performed calculations of $|\Re(\theta)|^2$ for a range of incidence angles θ and various values of water temperature and salinity which are the two most important driving parameters of the complex dielectric permittivity ε of sea water. The latter can be calculated using either the Klein and Swift model [18. 19], or Meissner and Wentz model [20]. Those models for the sea water permittivity rely on L-band measurements. They are close enough to each other at those frequencies, and no other models have been shown more reliable [21]. The analytical expressions for ε as a function of radio frequency, water temperature T and salinity S for the Klein and Swift model is given in Appendix to this Section. The radio frequency of the received signals for CYGNSS is known with high accuracy. It is the L1-band frequency which is equal to 1.57542 GHz. Figs. 4.1a and 4.b demonstrate the dependence of both the real and imaginary parts of the dielectric permittivity of ocean water (ε′ and ε′′, respectively) on water temperature and salinity.

Therefore, the retrieval of MSS depends on sea surface temperature (SST) and sea surface salinity (SSS). Analyses reveal that the changes in SSS and SST over time and space are small enough that using a single value of $|\Re(\theta)|^2$ maintains an acceptable error tolerance (Figure 4.2). Therefore, LUTs for monthly and zonal averaged Fresnel coefficients, at a 1° x 1° resolution, are used for the derivation of MSS (see Figure 4.3).

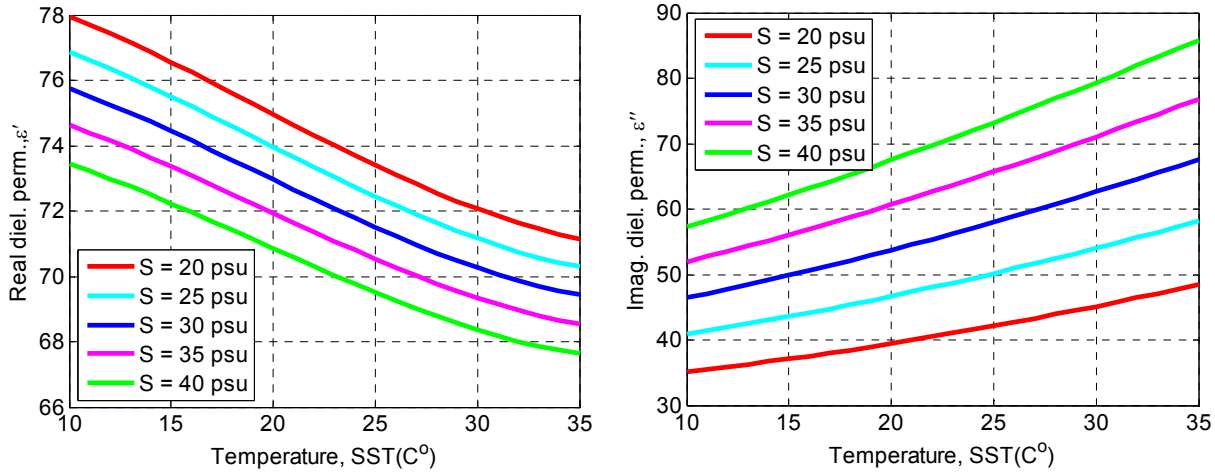

(a) (b)

Fig. 4.1. Dependence of both real and imaginary parts of dielectric permittivity of ocean water (ε′ and ε″, respectively) on water temperature and salinity.

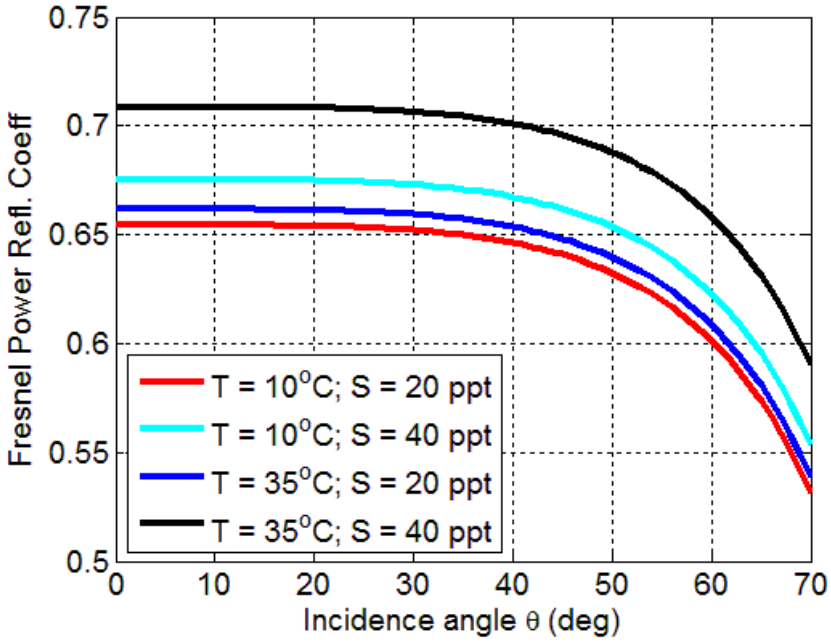

Fig. 4.2. Dependence of $|\Re(\theta)|^2$ on incidence angle for a wide range of temperatures and salinities calculated using the Klein and Swift model [18], [19].

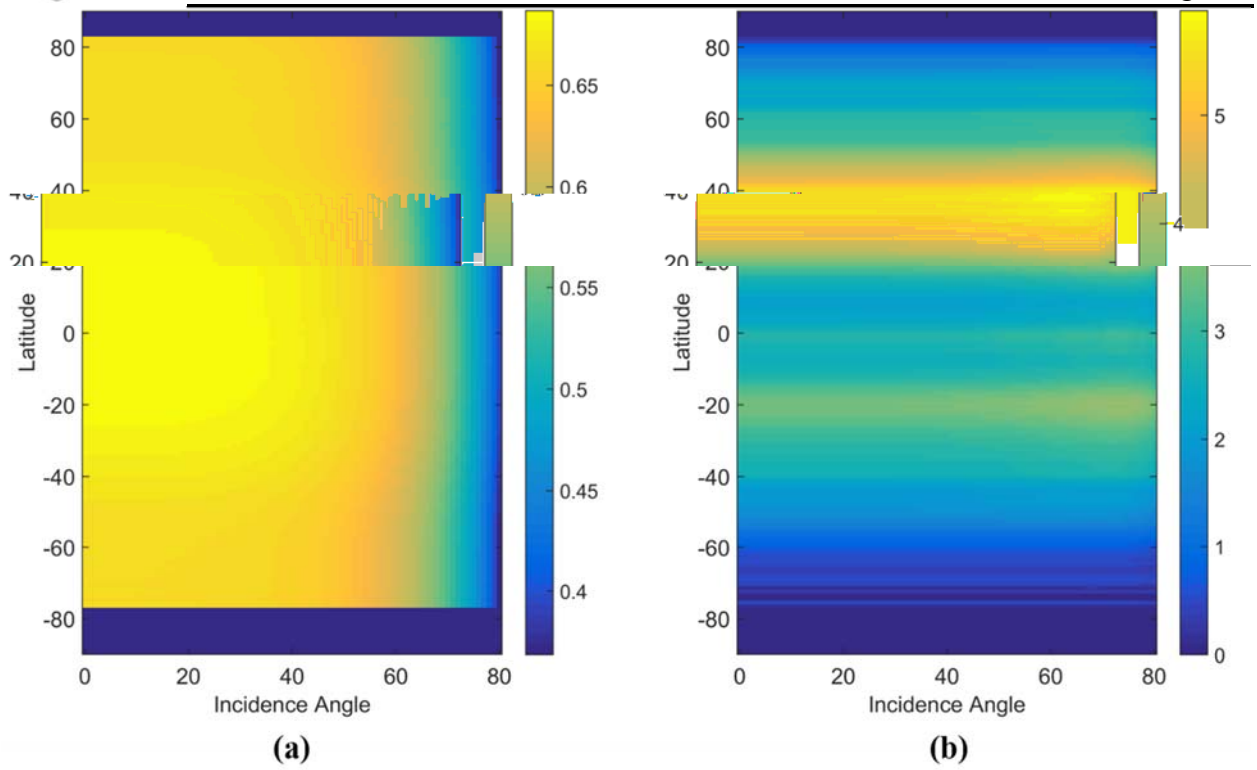

Fig. 4.3. (a) Average (zonal and seasonal) Fresnel reflection coefficient $|\Re(\theta)|^2$; (b) standard deviation (zonal and seasonal) of $|\Re(\theta)|^2$.

4.2. Error Analysis of the Level 2 MSS Retrieval Algorithm

The creation of the L2 MSS product is contingent on the availability of input observational data (from CYGNSS and ancillary data sources) and accurate estimates of their errors. The accuracy of the L2 MSS product is dependent on the accuracy of the BRCS σ_0 retrieval, the accuracy of the scattering geometry determination (incidence angle), and the accuracy of the Fresnel reflection coefficient estimates. It should be remembered that this algorithm is built upon two basic assumptions: validity of the Geometric Optics limit of the Kirchhoff approximation, and validity of the Gaussian PDF of slopes. At very rough surface conditions, such as in the hurricane wind maximum areas, both of these assumptions may be violated. These scenarios would require an independent calibration and validation of the MSS by using collocated and simultaneous in situ measurements of the MSS. In some circumstances, this may be impractical.

The expression for generating the Level 2 MSS data product is given by equation (3.8). The equation is repeated below with the reflection coefficient from (4.1) :

$$mss = \frac{\left|\Re(\theta)\right|^2}{\sigma_0(\theta)}. \tag{4.2}$$

Each uncertainty in the Level 2 MSS retrival algorithm will be considered as an independent uncorrelated error source. The total error in the Level 2 MSS retrieval is the root sum square (RSS) of individual errors contributed by the independent variable of (4.2). For relative MSS error we have:

$$\frac{\Delta mss}{mss} = \left[\sum_{i=1}^{4} E^2(p_i)\right]^{1/2}, \tag{4.3}$$

where the error variables are : $p_1 = \sigma_0(\theta)$, $p_2 = \theta$, $p_3 = T$, $p_4 = S$. The individual errors $E(p_i)$ can be expressed via partial derivatives as,

$$E(p_i) = \frac{1}{mss}\left|\frac{\partial mss}{\partial p_i}\right|\Delta p_i. \tag{4.4}$$

One can specify the error for each of these variables:

$$E(\sigma_0) = \frac{\left|\Re\right|^2}{\sigma_0}\left|\frac{\partial mss}{\partial \sigma_0}\right|\Delta\sigma_0 = \frac{\Delta\sigma_0}{\sigma_0}, \tag{4.5}$$

$$E(\theta) = \frac{\left|\Re\right|^2}{\sigma_0}\left|\frac{\partial mss}{\partial \theta}\right|\Delta\theta = \frac{1}{\left|\Re\right|^2}\left|\frac{\partial\left|\Re\right|^2}{\partial\theta}\right|\Delta\theta, \tag{4.6}$$

$$E(T) = \frac{\left|\Re\right|^2}{\sigma_0}\left|\frac{\partial mss}{\partial T}\right|\Delta T = \frac{1}{\left|\Re\right|^2}\left|\frac{\partial\left|\Re\right|^2}{\partial T}\right|\Delta T, \tag{4.7}$$

$$E(S) = \frac{\left|\Re\right|^2}{\sigma_0}\left|\frac{\partial mss}{\partial S}\right|\Delta S = \frac{1}{\left|\Re\right|^2}\left|\frac{\partial\left|\Re\right|^2}{\partial S}\right|\Delta S. \tag{4.8}$$

To estimate $E(\sigma_0)$, empirically derived values for σ_0 and $\Delta\sigma_0$, based on tests under different wind speeds, are employed. The error estimates for σ_0 also include uncertainties related to the antenna gain model, the LNA noise model, the GPS transmitter model, etc. For details see [17]:

$\sigma_0 = 20$ dB (100) and $\Delta\sigma_0 = 0.82$ dB (1.21), for $U_{10} < 20$ m/s;
$\sigma_0 = 12$ dB (15.85) and $\Delta\sigma_0 = 0.70$ dB (1.17), for U10 > 20 m/s.

Partial derivatives of $|\Re|^2$ in (4.6-4.8) are computed numerically because the analytical derivation is not practical due to a complicated dependence of $|\Re|^2$ over the arguments θ, T, and S. Examples of such computations are shown in Figures 4.4-4.6.

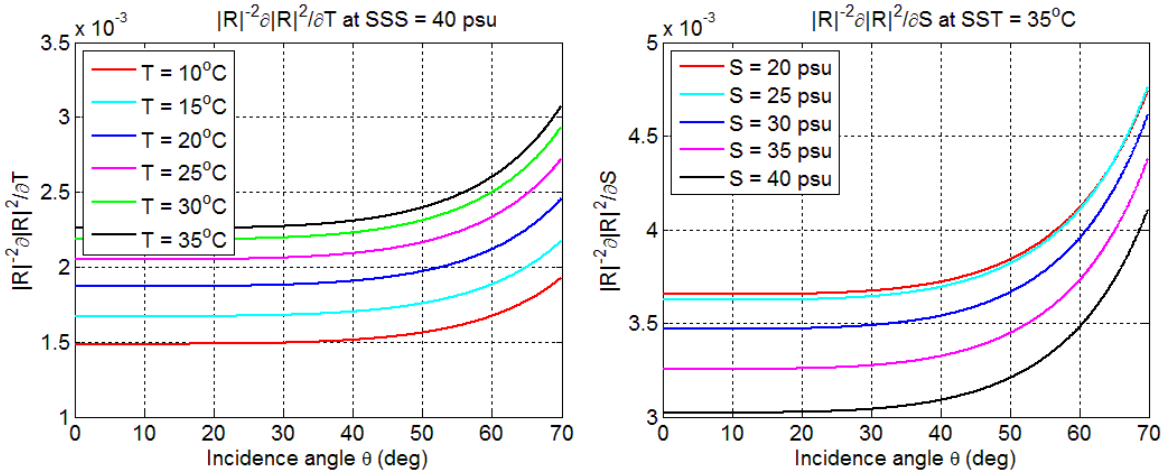

(a) (b)

Fig. 4.4. Relative partial derivatives of $|\Re|^2$ over temperature and salinity as a function of incidence angle.

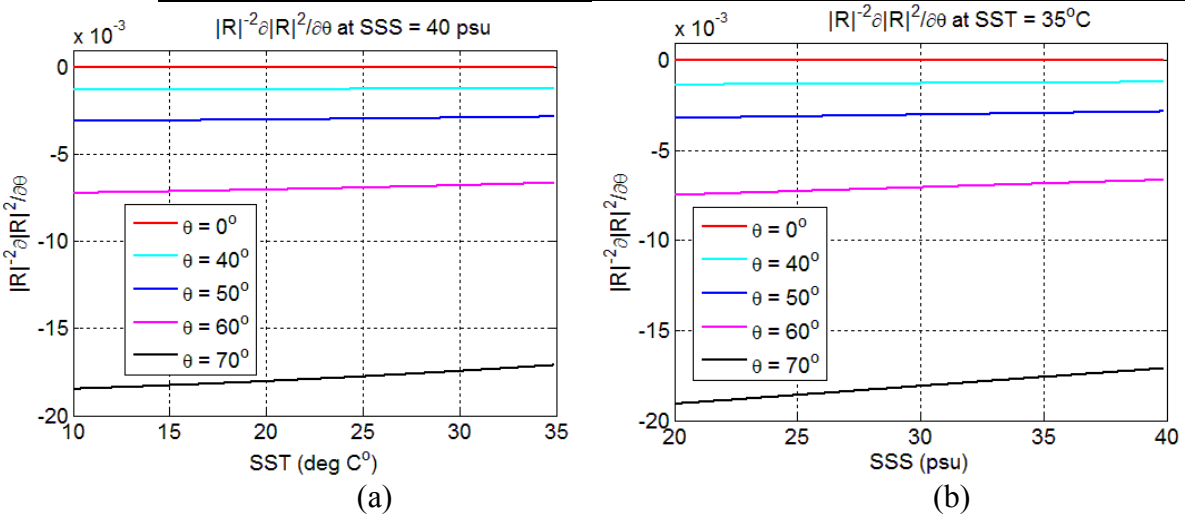

Fig. 4.5. Relative partial derivative of $|\Re|^2$ over incidence angle as a function of temperature and salinity.

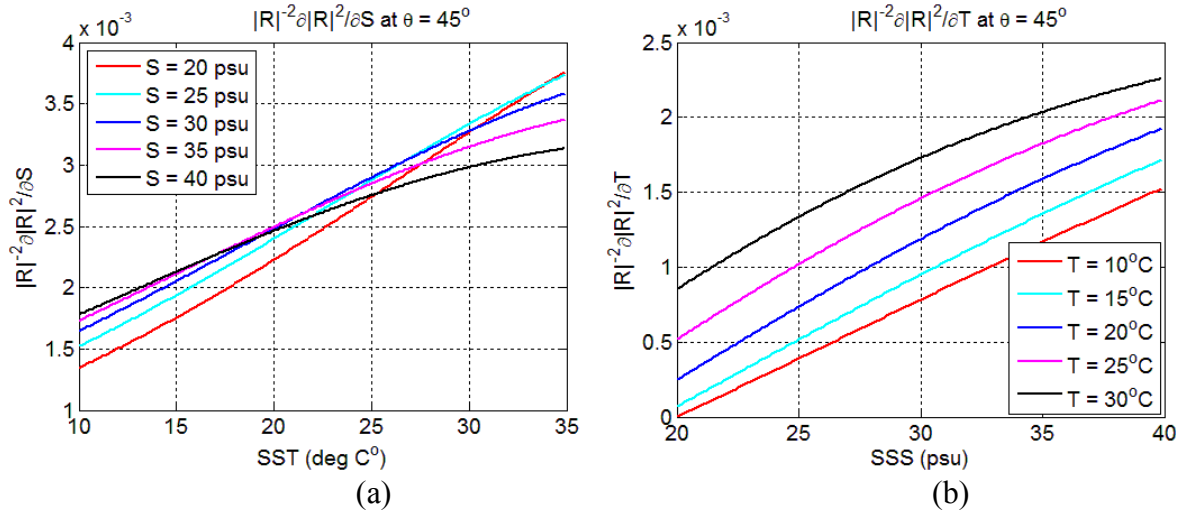

Fig. 4.6. Relative partial derivative of $|\Re|^2$ over temperature and salinity.

Fig. 4.4a represents $\frac{1}{|\Re|^2}\left|\frac{\partial|\Re|^2}{\partial T}\right|$ as a function incidence angle θ for a range of sea surface temperatures T between 10 ºC and 35ºC and for a fixed sea surface salinity $S = 40$ psu. Fig. 4.4b shows $\frac{1}{|\Re|^2}\left|\frac{\partial|\Re|^2}{\partial S}\right|$ as a function incidence angle θ for a range of sea surface salinities S between 10 and 40 psu and for a fixed sea surface temperature $T = 35$ºC. Analogously, Figs. 4.5a and 4.5b

represent respectively the dependence of $\frac{1}{|\Re|^2}\left|\frac{\partial|\Re|^2}{\partial\theta}\right|$ on temperature and salinity at fixed salinity and temperature for a range of incidence angles θ. And finally, Figs. 4.6a and 4.6b show cuts of functions $\frac{1}{|\Re|^2}\left|\frac{\partial|\Re|^2}{\partial S}\right|$ and $\frac{1}{|\Re|^2}\left|\frac{\partial|\Re|^2}{\partial T}\right|$ along parameters such as temperature and salinity keeping other parameters constant. All these plots give an idea of the relative magnitudes of values of quantities entering Eqs. (4.5) – (4.8). To obtain values of respective errors, $E(\sigma_0)$, $E(\theta)$, $E(T)$, and $E(S)$, one needs to input errors for $\Delta\sigma_0$, $\Delta\theta$, ΔT, and ΔS. In the following Tables we present results of calculations of the relative MSS error, $\frac{\Delta mss}{mss}$ based on (4.3-4.8) for some limiting values of the parameters involved.

TABLE 1. RELATIVE MSS ERROR (U_{10} < 20 m/s, $\Delta\sigma_0$ = 1.21, Δθ = 0.5°, ΔT = 0.5°C, ΔS = 2 psu)

Parameters	θ = 0°	θ = 35°	θ = 70°
SSS=20 psu, SST=10°C	$1.24\cdot10^{-2}$	$1.24\cdot10^{-2}$	$1.58\cdot10^{-2}$
SSS=40 psu, SST=10°C	$1.26\cdot10^{-2}$	$1.26\cdot10^{-2}$	$1.59\cdot10^{-2}$
SSS=20 psu, SST=35°C	$1.41\cdot10^{-2}$	$1.41\cdot10^{-2}$	$1.81\cdot10^{-2}$
SSS=40 psu, SST=35°C	$1.36\cdot10^{-2}$	$1.36\cdot10^{-2}$	$1.70\cdot10^{-2}$

TABLE 2. RELATIVE MSS ERROR (U_{10} > 20 m/s, $\Delta\sigma_0$ = 1.17, Δθ = 0.5°, ΔT = 0.5°C, ΔS = 2 psu)

Parameters	θ = 0°	θ = 35°	θ = 70°
SSS=20 psu, SST=10°C	$7.42\cdot10^{-2}$	$7.42\cdot10^{-2}$	$7.42\cdot10^{-2}$
SSS=40 psu, SST=10°C	$7.42\cdot10^{-2}$	$7.42\cdot10^{-2}$	$7.43\cdot10^{-2}$
SSS=20 psu, SST=35°C	$7.45\cdot10^{-2}$	$7.45\cdot10^{-2}$	$7.48\cdot10^{-2}$
SSS=40 psu, SST=35°C	$7.44\cdot10^{-2}$	$7.44\cdot10^{-2}$	$7.46\cdot10^{-2}$

TABLE 3. RELATIVE MSS ERROR (U_{10} < 20 m/s, $\Delta\sigma_0$ = 1.21, Δθ = 1°, ΔT = 1°C, ΔS = 5 psu)

Parameters	θ = 0°	θ = 35°	θ = 70°
SSS=20 psu, SST=10°C	$1.37\cdot10^{-2}$	$1.38\cdot10^{-2}$	$2.42\cdot10^{-2}$
SSS=40 psu, SST=10°C	$1.49\cdot10^{-2}$	$1.50\cdot10^{-2}$	$2.48\cdot10^{-2}$
SSS=20 psu, SST=35°C	$2.19\cdot10^{-2}$	$2.21\cdot10^{-2}$	$3.28\cdot10^{-2}$
SSS=40 psu, SST=35°C	$1.95\cdot10^{-2}$	$1.96\cdot10^{-2}$	$2.95\cdot10^{-2}$

TABLE 4. RELATIVE MSS ERROR (U_{10} > 20 m/s, $\Delta\sigma_0$=1.17, $\Delta\theta$ = 1°, ΔT = 1°C, ΔS = 5 psu)

Parameters	θ = 0°	θ = 35°	θ = 70°
SSS=20 psu, SST=10°C	$7.44\cdot10^{-2}$	$7.44\cdot10^{-2}$	$7.46\cdot10^{-2}$
SSS=40 psu, SST=10°C	$7.47\cdot10^{-2}$	$7.47\cdot10^{-2}$	$7.50\cdot10^{-2}$
SSS=20 psu, SST=35°C	$7.65\cdot10^{-2}$	$7.66\cdot10^{-2}$	$7.81\cdot10^{-2}$
SSS=40 psu, SST=35°C	$7.58\cdot10^{-2}$	$7.58\cdot10^{-2}$	$7.71\cdot10^{-2}$

For Tables 1 and 2 we used some reasonable values for input errors shown in the header of the table. One can see that the relative MSS error for U_{10} < 20 m/s, and for the range of incidence angles between 0 and 70°, lies within 1.7%, and within 7.5% for higher winds. The maximum relative MSS errors increase to 3% and 7.7% respectively, if a more conservative estimate is taken for the input errors shown in the header of Tables 3 and 4. The following conclusions can be drawn from these numbers. For winds below 20 m s^{-1} the MSS error is relatively low but it is more sensitive to the input SST and SSS errors, whereas for higher winds the MSS error is higher but is less sensitive to the input SST and SSS errors.

4.3 MSS Uncertainty Algorithm Implementation

As shown in Section 4.2, the dominant source of error in MSS is the uncertainty in measurement of the BRCS, σ_o. The sensitivity of MSS to the uncertainty in the Fresnel reflection coefficient, $\mathcal{R}$, is second order and will be neglected for purposes of the uncertainty algorithm implementation. Using this simplification, the uncertainty in MSS can written is

$$\Delta MSS = \frac{\Delta\sigma_o MSS}{\sigma_o} \tag{4.9}$$

where the three terms on the right in eqn. (4,9) are found by

$\Delta\sigma_o$ The uncertainty in BRCS, σ_o, as reported by the L1b algorithm for the central DDM in the time average.

MSS The L2 MSS data product given by eqn. (4.2)

σ_o The L1b DDMA observable for the central DDM in the time average used to compute the MSS. Specifically, it is calculated as sigma_DDMA/area_DDMA

4.4 Overall Uncertainty

Above we considered errors in determining the MSS due to thermal and speckle noise assuming that the MSS remains constant within the scene. This is only part of the uncertainty in the MSS retrieval. There are other factors which can add to the overall uncertainty.

There are factors related to the variability of the transmit signal and of the parameters of the receiving system. All of them can be boiled down to an uncertainty in the coefficient α introduced

above in (3.6-3.7). The coefficient is needed to calculate MSS from σ_0 measured in the specular direction. The uncertainty in the physical and technical parameters composing it can be eliminated, or significantly reduced, by calibration procedures, or by ancillary measurements. These procedures are described in [17].

First, the most important uncertainty is in the spatial variability of the MSS field. Even given a homogenous wind field, which is an input for the MSS, the wave statistics can be affected by limited fetch, swell, currents, surfactants, and bathymetry. If the scales of this spatial variability are smaller than or close to the spatial resolution of the system this factor can affect the accuracy of the MSS retrieval.

Our retrieval algorithm is based on Eq.(3.8) which, in turn, is based on the radar bistatic equation and diffusive rough surface described by the Geometric Optics limit of the Kirchhoff approximation and Gaussian PDF of surface slopes [1]. This equation and underlying EM scattering model work well for a broad range of surface conditions, but of course, they have their own limitations. If diffraction effects become important this model can be augmented by the Small Slope Approximation [24]. For the case of very small MSS < 0.003 (which correspond to very weak winds, U < 3m/s) the bistatic radar equation should be augmented by an additional coherent term [25]. The case of very steep and breaking waves can be challenging for the MSS retrieval based on either GO or the SSA, but in this case the notion of the MSS itself becomes questionable.

Appendix. Klein-Swift Ocean Dielectric Model

According to the empirical model of Klein and Swift [18] the real and imaginary parts of the dielectric constant of sea water at microwave frequencies are respectively:

$$\mathrm{Re}\,\varepsilon = \varepsilon_\infty + \left(\varepsilon_s - \varepsilon_\infty\right)/\left(1+\omega^2\tau^2\right) \qquad \text{(A1)}$$

and

$$\mathrm{Im}\,\varepsilon = \omega\tau\left(\varepsilon_s - \varepsilon_\infty\right)/\left(1+\omega^2\tau^2\right) + \sigma/\varepsilon_0\omega\,. \qquad \text{(A2)}$$

Here, $\omega = 2\pi f\cdot 10^9$ is the radian frequency (rad/s), and f is frequency in GHz;

$\varepsilon_0 = 8.854\cdot 10^{-12}$ is the dielectric permittivity of free space in farads/meter. $\varepsilon_\infty = 4.9$ is the dielectric permittivity of water at infinite frequency; $\varepsilon_s = a\varepsilon_{sT}$ is the static dielectric constant,

where

$$a = 1 + 1.613\cdot 10^{-5} TS - 3.656\cdot 10^{-3} S + 3.210\cdot 10^{-5} S^2 - 4.232\cdot 10^{-7} S^3, \qquad \text{(A3)}$$

$$\varepsilon_{sT} = 87.134 - 1.949\cdot 10^{-1} T - 1.276\cdot 10^{-2} T^2 + 2.491\cdot 10^{-4} T^3\,. \qquad \text{(A4)}$$

$\sigma = \sigma_0 \exp\left(-\Delta\beta\right)$ is the ionic conductivity in mhos/meter, where

$$\sigma_0 = S\left(0.182521 - 1.46192\cdot 10^{-3} S + 2.09324\cdot 10^{-5} S^2 - 1.28205\cdot 10^{-7} S^3\right), \qquad \text{(A5)}$$

and $\Delta = 25 - T$,

$$\beta = 2.033 \cdot 10^{-2} + 1.266 \cdot 10^{-4} \Delta + 2.464 \cdot 10^{-6} \Delta^2 - S\left(1.849 \cdot 10^{-5} - 2.551 \cdot 10^{-7} \Delta + 2.551 \cdot 10^{-8} \Delta^2\right). \quad \text{(A5)}$$

Here, S is sea water salinity in parts per thousand, T is sea water temperature in C^o.

$\tau = b\tau_0$ is the relaxation time in seconds, where

$$b = 1 + 2.282 \cdot 10^{-5} ST - 7.638 \cdot 10^{-4} S - 7.760 \cdot 10^{-6} S^2 + 1.105 \cdot 10^{-8} S^3, \quad \text{(A6)}$$

and

$$\tau_0 = 1.768 \cdot 10^{-11} - 6.086 \cdot 10^{-13} T + 1.104 \cdot 10^{-14} T^2 - 8.111 \cdot 10^{-17} T^3. \quad \text{(A7)}$$

5. References

1. Zavorotny, V. U., and A. G. Voronovich, 2000: Scattering of GPS signals from the ocean with wind remote sensing application. *IEEE Trans. Geosci. Remote Sens.*, **38**, 951–964.
2. Jähne, B., K. O. Münnich, R. Bösinger, A. Dutzi, W. Huber and P. Libner, 1987: On the parameters influencing air-water gas exchange. *J. Geophys. Res.*, **92**, 1937–1949, 1987.
3. Wu, J., 1990: Mean square slopes of the wind-disturbed water surface, their magnitude, directionality and composition. *Radio Sci.*, **25**, 37–48.
4. Liu, Y., X. H. Yan, W. T. Liu, and P. A. Hwang, 1997: The probability density function of ocean surface slopes and its effects on radar backscatter. *J. Phys. Oceanogr.,* **27,** 782–797.
5. Walsh, E. J., D. C. Vandemark, C. A. Friehe, S. P. Burns, D. Khelif, R. N. Swift, and J. F. Scott, 1998: Measuring sea surface mean square slope with a 36-GHz scanning radar altimeter. *J. Geophys.Res.,* **103,** 12 587–12 601.
6. Chapron, B.,V. Kerbaol, D. Vandemark, and T. Elfouhaily, 2000: Importance of peakedness in sea surface slope measurements and applications. *J. Geophys. Res.,* **105,** 17 195–17 202.
7. Y. Liu, M-Y. Su, X-H. Yan, W. T. Liu, 2000: The mean-square slope of ocean surface waves and its effects on radar backscatter. *J. Atmos. Oceanic Technol.***, 17**, 1092–1105.
8. J. Font, G. Lagerloef, D. LeVine, A. Camps, and O. Z. Zanife, 2004: The determination of surface salinity with the European SMOS space mission. *IEEE Trans. Geosci. Remote Sens.*, **42**, no. 10, 2196–2205.
9. Guimbard, S., J. Gourrion, M. Portabella, A. Turiel, C. Gabarró, and J. Font, 2012: SMOS semi-empirical ocean forward model adjustment. *IEEE Trans. Geosci. Remote Sens.*, **50**, no. 5, 1676–1686.
10. Bass, F. G. and I. M. Fuks, 1979: *Wave Scattering From Statistically Rough Surfaces*. New York: Pergamon.
11. Barrick, D. E., 1968: Relationship between slope probability density function and the physical optics integral in rough surface scattering. *Proc. IEEE*, **56**, 1728–1729.
12. Elfouhaily T., D.R. Thompson and L. Lindstrom, 2002: Delay-Doppler analysis of bistatically reflected signals from the ocean surface: theory and application. *IEEE Trans. Geosci. Remote Sens.*, **40**, no. 3, 560–573.
13. Soulat, F., *Sea Surface Remote Sensing With GNSS and Sunlight Reflections*. Ph.D. Thesis. Universitat Politecnica de Catalunya, 2004.Cardellach, E., and A. Rius, 2008: A new technique to sense non-Gaussian features of the sea surface from L-band bistatic GNSS reflections. *Remote Sens. Environ.*, **112**, 2927–2937.
14. Cardellach, E., and A. Rius, 2008: A new technique to sense non-Gaussian features of the sea surface from L-band bistatic GNSS reflections. *Remote Sens. Environ.*, **112**, 2927–2937.
15. Elfouhaily, T., B. Chapron, K. Katsaros, and D. Vandemark, 1997: A unified directional spectrum for long and short wind-driven waves. *J. Geophys. Res.*, **102**, 15 781–15 796.
16. Cox, C., and W. Munk, 1954: Measurement of the roughness of the sea surface from photographs of the Sun's glitter. *J. Opt. Soc. Am.,* **44**, 835–850.

17. Gleason, S., 2013: CYGNSS DDM Calibration: General Level 1A and 1B Data Products. *Algorithm Theoretical Basis Documents*, Univ. of Michigan.
18. Klein, L. A., and C.T. Swift, 1977: An improved model for the dielectric constant of sea water at microwave frequencies. *IEEE Trans. Antennas Propag*., **AP-25**, 104–111.
19. Ulaby, F. T, R. K. Moore, and A. K. Fung. *Microwave Remote Sensing*, Artech House, 1986, vol.III, pp.2022–2025.
20. Meissner, T., and F. J. Wentz, 2004: The complex dielectric constant of pure and sea water from microwave satellite observations. *IEEE Trans. Geosci Remote Sens*., 42, 1836–1849.
21. Ellison, W., A. Balana, G. Delbos, K. Lamkaouchi, L. Eymard, C. Guillou, and C. Prigent, 1998: New permittivity measurements of sea water, *Radio Sci.*, **33**, 639–648.
22. Katzberg, S. J., O. Torres, and G. Ganoe, 2006: "Calibration of reflected GPS for tropical storm wind speed retrievals," *Geophys. Res. Lett.*, **33**, L18602, doi:10.1029/2006GL026825.
23. Level 2 Wind Speed Retrieval. *Algorithm Theoretical Basis Documents*, Univ. of Michigan, Dec. 2013.
24. Voronovich A. G., and V. U. Zavorotny, 2014: "Full-polarization modeling of monostatic and bistatic radar scattering from a rough sea surface," *IEEE Trans. Antennas Propag*., **62**, no. 3, 1363–1371.
25. Zavorotny, V. U., Gleason, S., Cardellach, E., & Camps, (2014). A. Tutorial on remote sensing using GNSS bistatic radar of opportunity, *Geoscience and Remote Sensing, IEEE Magazine*, *2*(4), 8-45. DOI: 10.1109/MGRS.2014.2374220